

Geophysical Research Letters[®]

RESEARCH LETTER

10.1029/2022GL097745

Key Points:

- A teleconnection exists between the Antarctic sea ice anomalies and the sea-surface-temperature anomaly known as the Indian Ocean Basin Mode (IOBM)
- The IOBM and Antarctic sea ice connection varies spatially and seasonally, is stronger in autumn and spring, and is modulated by El Niño-Southern Oscillation (ENSO)
- Removing the ENSO modulation, the extent of sea ice concentration anomalies shrinks a lot, and the source of the wavetrain moves westward

Supporting Information:

Supporting Information may be found in the online version of this article.

Correspondence to:

L. Yu,
yulejiang@sina.com.cn

Citation:

Yu, L., Zhong, S., Vihma, T., Sui, C., & Sun, B. (2022). The impact of the Indian Ocean Basin mode on Antarctic sea ice concentration in interannual time scales. *Geophysical Research Letters*, 49, e2022GL097745. <https://doi.org/10.1029/2022GL097745>

Received 9 JAN 2022

Accepted 20 MAY 2022

© 2022. American Geophysical Union.
All Rights Reserved.

The Impact of the Indian Ocean Basin Mode on Antarctic Sea Ice Concentration in Interannual Time Scales

Lejiang Yu¹ , Shiyuan Zhong² , Timo Vihma³ , Cuijuan Sui⁴, and Bo Sun¹

¹MNR Key Laboratory for Polar Science, Polar Research Institute of China, Shanghai, China, ²Department of Geography, Environment and Spatial Sciences, Michigan State University, East Lansing, MI, USA, ³Finnish Meteorological Institute, Helsinki, Finland, ⁴National Marine Environmental Forecasting Center, Beijing, China

Abstract The Antarctic sea ice variability has been linked to tropical sea surface temperature. However, little is known as to whether and how the Indian Ocean Basin Mode (IOBM) influences Antarctic sea ice changes. We revealed the existence of a teleconnection between the IOBM and Antarctic sea ice anomalies, which is much stronger in austral spring and autumn than summer and winter. In particular, under the positive phase of the IOBM, significant positive sea ice anomalies occur in the Bellingshausen and northern Weddell Seas, in contrast to negative anomalies in the Amundsen Sea, the southern Atlantic Ocean, and the coastal seas off Dronning Maud Land. This teleconnection is established by planetary wavetrains excited over the tropical Indian Ocean and the tropical Pacific Ocean and is modulated by El Niño-Southern Oscillation. The IOBM-related Antarctic sea ice anomalies are largely consistent with those of the anomalous surface air temperature and wind fields associated with the IOBM.

Plain Language Summary The variability of sea surface temperature in the tropical Indian Ocean is dominated by two modes, the Indian Ocean Dipole (IOD) and the Indian Ocean Basin Mode (IOBM). While previous studies have linked IOD to Antarctic sea ice changes, little is known about whether and how IOBM may affect seasonal Antarctic sea ice. Using 40-year (1979–2018) observational and reanalysis data, we found that there exists a significant teleconnection between the IOBM and the Antarctic sea ice anomalies in austral autumn and spring, and that this remote connection can be largely explained by anomalous atmospheric circulations.

1. Introduction

As an important component of the global climate system, the Antarctic sea ice exerts large effects on a range of southern mid-latitude atmosphere and ocean features including storm tracks (Kidston et al., 2011), mesoscale cyclones (Uotila et al., 2011), ocean surface energy balance (Vihma et al., 2009), top-of-the-atmosphere energy balance (Riihelä et al., 2021), carbon uptake (Delille et al., 2014), and formation of the deepest water masses in the Southern Ocean (Kerr et al., 2018). Further, land-fast sea ice acts as an important dynamical buffer between the ocean and the ice sheet/ice shelves (Massom et al., 2018), and thus indirectly affects sea level rise. The variability and changes of the Antarctic sea ice are influenced by a variety of climate drivers (Hobbs et al., 2016). Among the known climate variability modes, the Southern Annular Mode (SAM) has been identified as a key driver for the Antarctic sea ice variability across a range of time scales from seasonal to decadal; the positive (negative) SAM phase corresponds to the negative (positive) sea ice anomalies in the Weddell Sea, and the opposite is true in the Ross Sea (Kwok & Comiso, 2002; Lefebvre & Goosse, 2005; Zhang et al., 2018). On the interannual time scale, the eastern Pacific El Niño (La Niña) events appear to be associated with negative (positive) sea ice anomalies in the South Pacific (South Atlantic) (Yuan, 2004). The response of Antarctic sea ice to the phases of the El Niño-Southern Oscillation (ENSO) is modulated by the background state of the SAM (Fogt et al., 2010; Stammerjohn et al., 2008) and the relationship between the Antarctic sea ice and ENSO is stronger in austral winter and spring than summer and autumn (Simpkins et al., 2012). Raphael (2007) noted a significant relationship between the Zonal Wave Three mode and the Antarctic sea ice anomalies in austral autumn and early winter. In addition, the positive (negative) anomaly of the Amundsen Sea Low is related to more (less) sea ice cover in the Ross Sea and vice versa in the Antarctic Peninsula/Bellingshausen Sea (Turner et al., 2016).

Besides the sea surface temperature (SST) anomalies in the Pacific and Atlantic Oceans, Antarctic sea ice changes have also been linked to the SST anomalies in the tropical Indian Ocean (TIO). One of the two dominant SST

variability modes in TIO, the Indian Ocean Dipole (IOD), is characterized by the Dipole Mode Index (DMI) calculated as the difference in SST anomaly between the western TIO (50°E–70°E, 10°S–10°N) and the south-eastern TIO (90°E–110°E, 10°S–0°) (Saji et al., 1999). IOD has been shown to exert its maximum effects on sea ice in the region west of the Ross Sea, and positive (negative) DMI corresponds to positive (negative) sea ice anomalies near 60°E and vice versa near 90°E (Nuncio & Yuan, 2015). Little is known, however, if the other dominant TIO mode, the Indian Ocean Basin Mode (IOBM), is also related to the Antarctic sea ice variability. The IOBM, which represents uniform SST variability across the TIO on interannual time scale (Chambers et al., 1999; Klein et al., 1999; Saji et al., 1999), displays a close relationship with ENSO (Schott et al., 2009; Xie et al., 2016). Specifically, a boreal wintertime El Niño event is often a precursor to the positive phase of the IOBM in the subsequent boreal spring (Wang et al., 2019). According to Klein et al. (1999) and Saji et al. (1999), the IOBM is entirely forced by ENSO, whereas Wang et al. (2019) specified that the boreal wintertime El Niño event may produce the positive phase of the IOBM in the subsequent boreal spring. However, Taschetto et al. (2011) found that part of the IOBM signal does remain after the ENSO forcing is removed.

Xie et al. (2009, 2016) coined the effect of the IOBM on the tropical Pacific climate as “the Indian Ocean capacitor effect.” As such, the positive phase of the IOBM in boreal winter and spring, following an El Niño event, in turn influences summer northwestern Pacific climate through a baroclinic Kelvin wave into the Pacific (Xie et al., 2016). The interannual variability of the IOBM index has been linked to the boreal summer climate variability (Li et al., 2008; Xie et al., 2016; Yang et al., 2009). In addition, the IOBM can drive strong subsidence over Australia, prolonging the January–March dry conditions associated with El Niño events (Taschetto et al., 2011). Taschetto and Ambrizzi (2012) and de Souza et al. (2021) noted that the IOBM can modulate the March–May rainfall in South America via an anomalous Walker circulation and a mid-latitude wavetrain.

Although the IOBM has been linked to the Southern Hemisphere extratropical climate, its relationship with Antarctic sea ice remains to be investigated. In this study, we shall explore the linkage of the IOBM to the Antarctic sea ice concentration for each season and examine how the relationship is modulated by the presence/absence of the ENSO signal.

2. Data Set and Methods

The monthly SST data used in this study are from the United States National Oceanic and Atmospheric Administration (NOAA) Extended Reconstructed SST V5 (Huang et al., 2017). The SST data have a horizontal resolution of 2.0° latitude × 2.0° longitude for the period from 1854 to the present. The empirical orthogonal function (EOF) analysis is performed for detrended (separately for each grid point) seasonal SST in the TIO (30°S–30°N, 40°–100°E) over the 1979–2018 period to obtain the IOBM index, which is defined as the time series of the first EOF mode (Sun et al., 2019). The spatial pattern of the IOBM for austral winter (Figure 1c, showing the positive phase of IOBM) is similar to that of Sun et al. (2019), though the strength of the warm anomaly center in the southwestern Indian Ocean is somewhat different, which may be due to the 1-month shift in the definition of Austral winter between ours (JAS) and theirs (JJA).

Our study shall examine whether some signals of sea ice anomalies related to the IOBM remain in the absence of the ENSO signal. The ENSO signal here is denoted by the Niño3.4 index, which refers to the SST anomalies in the region (5°N–5°S, 170°W–120°W), and is obtained from the NOAA's Climate Prediction Center. To remove the ENSO signal from the IOBM index for each season, a method proposed by An (2003) is utilized, which is based on the following formula:

$$IOBM^* = IOBM - Niño3.4 \times cov(IOBM, Niño3.4) / var(Niño3.4) \quad (1)$$

where *IOBM* and *IOBM** represent the time series of the IOBM index with and without the ENSO signal, respectively, *cov*(*IOBM*, *Niño3.4*) denotes the temporal covariance between *IOBM** and the Niño3.4 index, and *var*(*Niño3.4*) indicates the variance of the Niño3.4 index. Equation 1 is also used for removing the DMI signal from the IOBM.

The monthly sea ice concentration data from January 1979 to December 2018 are downloaded from the U.S. National Snow and Ice Data Center (NSIDC). The data are on a polar stereographic grid with 25-km spacing. The monthly atmospheric data from the European Centre for Medium-Range Weather Forecasts (ECMWF)

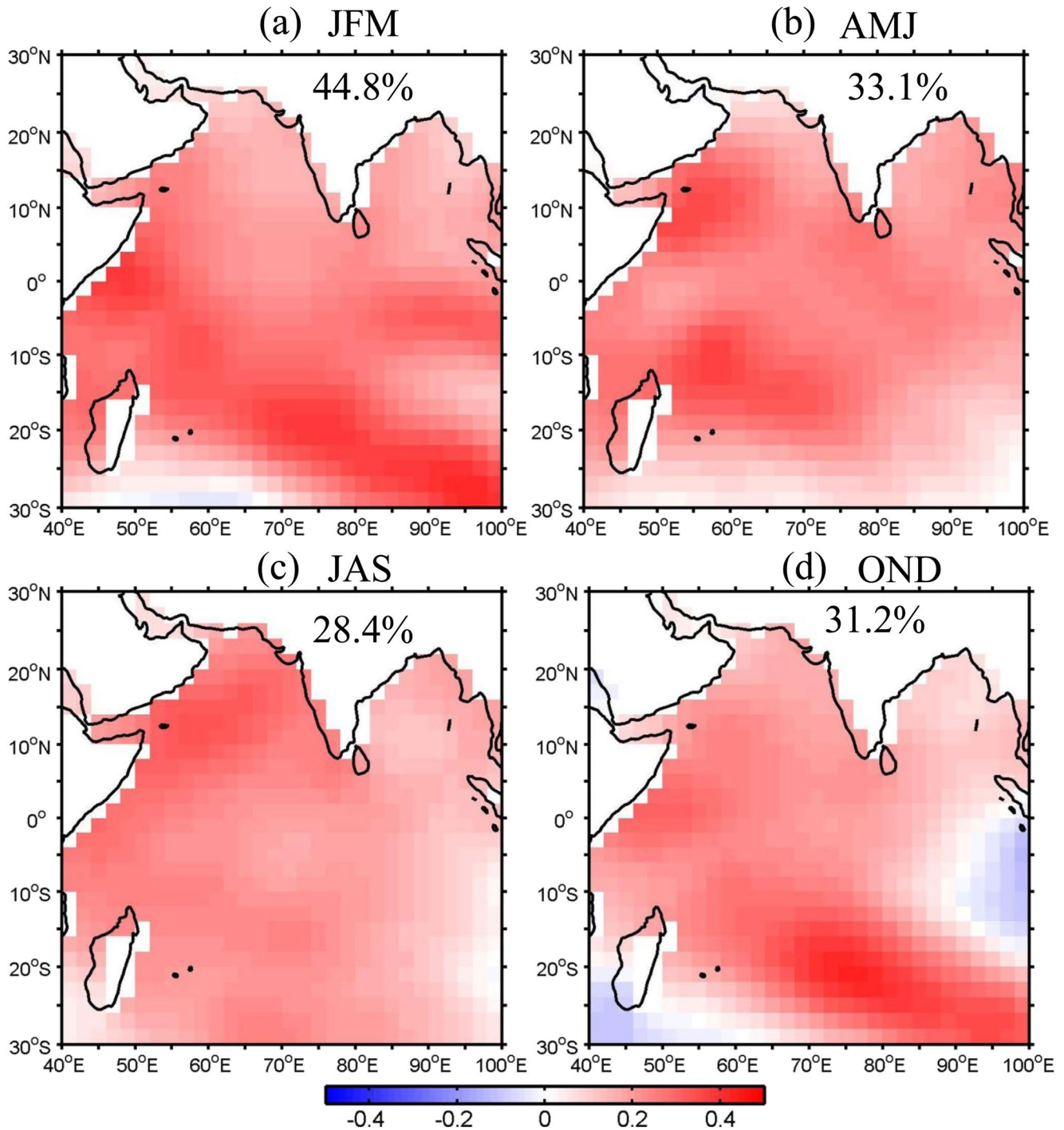


Figure 1. Spatial patterns of the first modes of detrended SST variability ($^{\circ}\text{C}$) over the tropical Indian Ocean for austral summer (JFM) (a), autumn (AMJ) (b), winter (JAS) (c), and spring (OND) (d). The percentage in each panel indicates the ratio of the total variance explained by the first modes.

fifth-generation reanalysis (ERA5, Hersbach et al., 2020) are utilized to explain the interannual variability of Antarctic sea ice associated with the IOBM index. The ERA5 data describe reasonably well the climate in southern mid and high latitudes (Gossart et al., 2019; Ramon et al., 2019). In addition, monthly outgoing longwave radiation (OLR) from the top of the atmosphere derived from NOAA Interpolated OLR data set (Liebmann & Simth, 1996) is also used in the analysis as a proxy for convective activities over tropical oceans. To describe the

generation and propagation of planetary waves, we utilize the Rossby wave source (RWS), following Sardeshmukh and Hoskins (1988), as well as wave activity flux described in Takaya and Nakamura (2001).

Other statistical analysis methods, besides EOF, include linear correlation and regression, for which the statistical significance on interannual time scales is determined by a two-tailed Student's t test assuming 40 independent samples. Before the correlation or regression analyses is applied to the data, the variables and indices are detrended. The analyses are performed for all four seasons, but we will focus our presentation on the results for austral autumn (April–June) and spring (October–December) when the relationship between the IOBM and the Antarctic sea ice concentrations are much stronger than the other two seasons. The results for austral summer (January–March) and winter (July–September) can be found in Supplemental Materials. Repeating the same analyses with a different sea ice data set and a reanalysis data set yielded similar results, indicating our results are not sensitive to the specific datasets chosen for the study.

3. Results

As the first EOF mode of the SST variability over the TIO, the IOBM explains 28.4%–44.8% of the total SST variance across the four seasons (Figure 1). The spatial patterns of the IOBM display positive SST anomalies nearly everywhere in the TIO, with the exception of the eastern portion in austral spring the southwestern portion in both spring and summer (Figure 1). The magnitude of the positive SST anomalies shows regional variability, with larger SST anomalies in the southeastern TIO in austral spring and summer, and in the western TIO in austral autumn and winter. Although there is a small region in the eastern TIO where the SST anomalies are negative in austral spring, the pattern is different from what was found previously during the positive phase of the IOD (Nuncio & Yuan, 2015) (Figure S1 in Supporting Information S1). The spatial pattern of the IOBM in austral winter (Figure 1c) is similar to the result of Sun et al. (2019), and the summer pattern (Figure 1a) is similar to those of Saji et al. (1999) and Taschetto et al. (2011) that used data from all months.

The IOBM index is correlated with the Niño3.4 index, with the correlation coefficient (r) varying between 0.37 in austral winter and 0.75 in austral summer, all significant at 95% confidence level (Table S1 in Supporting Information S1). Schott et al. (2009) suggested that the IOBM peaks in autumn and is strongly related to the decaying ENSO, which is consistent with the rather high autumn correlation ($r = 0.54$), although not the highest among the four seasons. There are significant correlations between the DMI and the IOBM indices in austral spring, as suggested by Abram et al. (2020) and Taschetto et al. (2011). The spatial pattern of the spring DMI resembles that of the IOBM index (Figure S1a in Supporting Information S1 and Figure 1d). We remove the DMI signal from the IOBM index in austral spring following Equation 1. The spatial pattern of the new IOBM index shows a uniform variability in the TIO (Figure S1b in Supporting Information S1). The new IOBM index also has a significant, albeit weak, correlation with the Niño3.4 index in spring ($r = 0.35$, $p < 0.05$). Although the spatial pattern of the DMI index in austral winter is not similar to that of the IOBM index (Figure S1c in Supporting Information S1 and Figure 1c), there is a significant correlation between the two indices. However, the new IOBM index for austral winter has no significant correlation with the winter Niño3.4 index ($r = 0.10$, $p > 0.05$). Hereafter, the IOBM refers to the original index for autumn and summer, but to the new index with the DMI signal removed for spring and winter. The second mode of SST variability over the TIO shows a dipole structure in austral summer and autumn and a tripole structure in austral winter and spring, and only explains 10%–16% of the total variance (Figure S2 in Supporting Information S1).

As significant correlations and interactions exist between the IOBM and the Niño3.4 indices, it is necessary to examine the relationships between the IOBM indices and the Antarctic sea ice concentration anomalies separately under conditions with and without the ENSO signal. To achieve this, we regress the seasonal sea ice concentration anomalies onto the seasonal detrended IOBM index with and without the ENSO signal, referring to *IOBM* and *IOBM** in Equation 1, respectively, and the results are shown for austral autumn (Figures 2a and 2b). Associated with the positive IOBM with the ENSO signal are significant positive sea ice concentration anomalies over the Bellingshausen and northern Weddell Seas and negative anomalies in the coastal seas off the Dronning Maud Land (Figure 2a). With the ENSO signal removed, the extent of the above-mentioned positive sea ice anomalies and the negative sea ice anomalies near 20°E is reduced substantially, but the coverage of the negative anomalies in the southern Indian Ocean is slightly expanded near 90°E and 10°W (Figure 2b). The ENSO modulation on the relationship between the IOBM and the Antarctic sea ice anomalies is further elucidated by comparing the

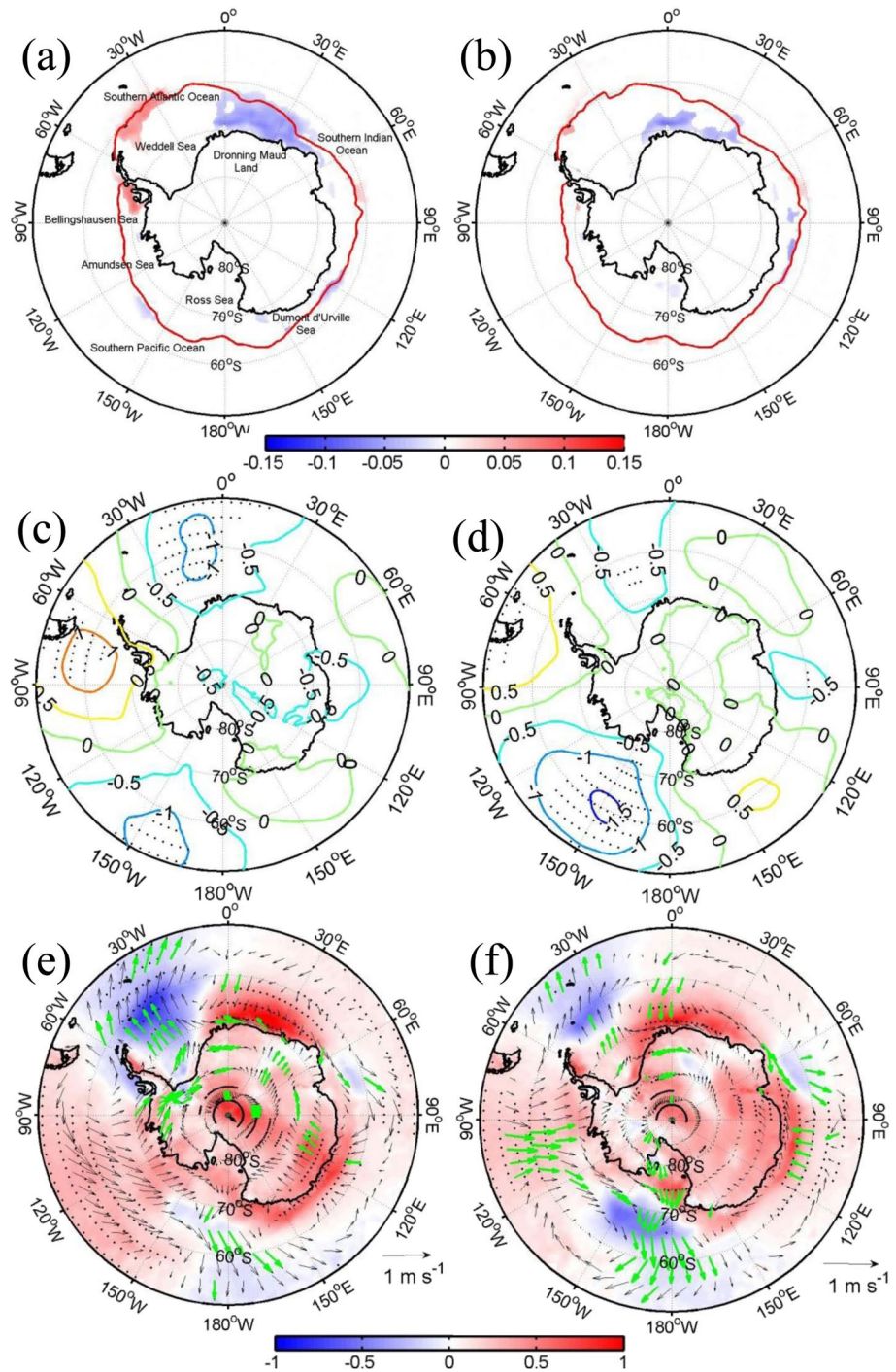


Figure 2. Regression map of anomalous seasonal sea ice concentration (a and b), mean sea level pressure (MSLP) (hectopascal) (c and d), and 10-m wind field (vector) and 2-m air temperature (°C) (e and f) onto the detrended Indian Ocean Basin Mode indices with the El Niño-Southern Oscillation (ENSO) signal (a, c and e) and without the ENSO signal (b, d and f) for austral autumn over the 1979–2018 period. Only results at above 90% confidence levels are shown in panels (a and b). Dotted regions denote above 90% confidence level for MSLP and surface air temperature in panels (b, d, e and f). Green vectors denote above 90% confidence level in panels (e and f). The red thick lines in panels (a and b) denote the climatological sea ice extent (sea ice concentration is equal to 0.15).

patterns above to the regression patterns of the Antarctic sea ice anomalies onto the Niño 3.4 index (Figure S3b in Supporting Information S1). Although the ENSO-related sea ice anomalies tend to have a larger spatial extent, particularly in autumn and winter, the spatial patterns are overall similar, suggesting that the relationship between the IOBM and the Antarctic sea ice anomalies is strongly modified by the presence or absence of ENSO.

To explain the spatial pattern of the sea ice concentration anomalies in austral autumn from the perspective of local factors, we perform a regression analysis, in which several atmospheric variables including anomalous mean sea level pressure (MSLP), surface (2 m) air temperature, surface (10 m) wind vector, and downward longwave radiation are regressed onto the IOBM index with and without the ENSO signal (Figures 2c–2f and S4 in Supporting Information S1). The MSLP regression reveals a structure of zonal wavenumber two over the Southern Ocean, with significant MSLP anomalies over the Atlantic and Pacific sectors (Figure 2c). The anomalous cyclonic (anticyclonic) circulation around the negative (positive) MSLP anomalies over the eastern Weddell Sea (the Bellingshausen Sea) produces anomalous southerly winds (Figure 2e), which push sea ice off shore, increasing the sea ice cover over the northern Weddell and Bellingshausen Seas (Figure 2a). Meanwhile, the cold advection associated with the anomalous southerly winds decreases 2-m air temperature (Figure 2e), which expands the sea ice cover over the northern Weddell and Bellingshausen Seas. The drier and colder air coincides with the negative downward longwave radiation anomalies (Figure S4a in Supporting Information S1), further decreasing surface temperature. The negative MSLP anomalies over the eastern Weddell Sea induce anomalous northerly winds over the eastern Atlantic sector of the Southern Ocean (Figure 2e), which reduces the sea ice cover at the coast of Dronning Maud Land. Positive surface air temperature anomalies related to anomalous southward heat transport and increasing downward longwave radiation anomaly also favor negative sea ice concentration anomalies. Such a response of Antarctic sea ice to the changes in the atmospheric circulations is in agreement with previous studies (Yu et al., 2018; Yu, Zhong, Sui, et al., 2021; Yu, Zhong, Vihma, et al., 2021).

Removing the effect of the ENSO signal, the structure of wavenumber two remains, but the strength and position of the anomaly centers have changed, as indicated by a significant strengthening of the low pressure over the Pacific sector (Figure 2d). The anomalous low-pressure centers over the eastern Atlantic sector also generate positive anomalies of the surface air temperature and negative anomalies of the sea ice concentration along the coast of Dronning Maud Land (Figures 2d and 2e). The negative sea ice concentration anomalies at the longitude of 90°E are also related to the anomalous low pressure and northerly winds there. Positive downward longwave radiation anomalies also are in favor of decreased sea ice cover (Figure S4c in Supporting Information S1).

Previous studies suggested that SST anomalies over the TIO can influence atmospheric circulation at southern mid-high latitudes (Hoskins & Karoly, 1981; McIntosh & Hendon, 2017; Nuncio & Yuan, 2015; Wang et al., 2019). To determine how ENSO may modulate the relationship between the IOBM and the mid-high latitude anomalous atmospheric circulations, several relevant atmospheric variables, including the 200-hPa geopotential height, OLR, wave activity flux, streamfunction, 200-hPa divergent wind, and RWS are regressed onto the austral autumn IOBM index with and without the ENSO signal (Figure 3). The regression of the 200-hPa geopotential height shows the structure of wave number two over the Southern Ocean (Figure 3e). The structure is associated with planetary wavetrains propagating southeastwards into the Southern Ocean (Figure 3e). The wavetrain is excited by the convective activities over the central and eastern Pacific Ocean (Figure 3a), which corresponds to the anomalous convergent wind and negative RWS in the subtropics to the east of Australia (Figure 3c). The removal of the ENSO signal does little to the spatial pattern of the 200-hPa geopotential height, but results in some changes in the strength and location of the anomaly centers (Figure 3f). The convective activities are weaker and they occur mainly over the Indian Ocean and western Pacific Ocean (Figure 3b). The RWS and convergent wind to the east of Australia also weaken considerably (Figure 3d). The wavetrain still exists, but its strength and location have changed (Figure 3f).

We now move on to show results for austral spring (Figures 4 and 5). Note that in the following analysis the DMI signal has been removed from the IOBM index using Equation 1 where the Niño3.4 index is replaced by the DMI index. The largest areas with significant (90% confidence level) regression of sea ice anomalies on the IOBM index occur in austral spring (Figure 4a). Positive IOBM with the ENSO signal is associated with positive sea ice anomalies in the Bellingshausen, Weddell, and Dumont d'Urville Seas, and negative ones in the Amundsen Sea, the Ross Sea and the southwestern Indian Ocean sector (30°E). Without the ENSO signal, the spatial extent of sea ice in the Southern Ocean related to the positive IOBM index decreases, but anomalous sea ice remains in the Weddell Sea and the southern Pacific Ocean (Figure 4b). The spatial pattern of the sea ice concentration

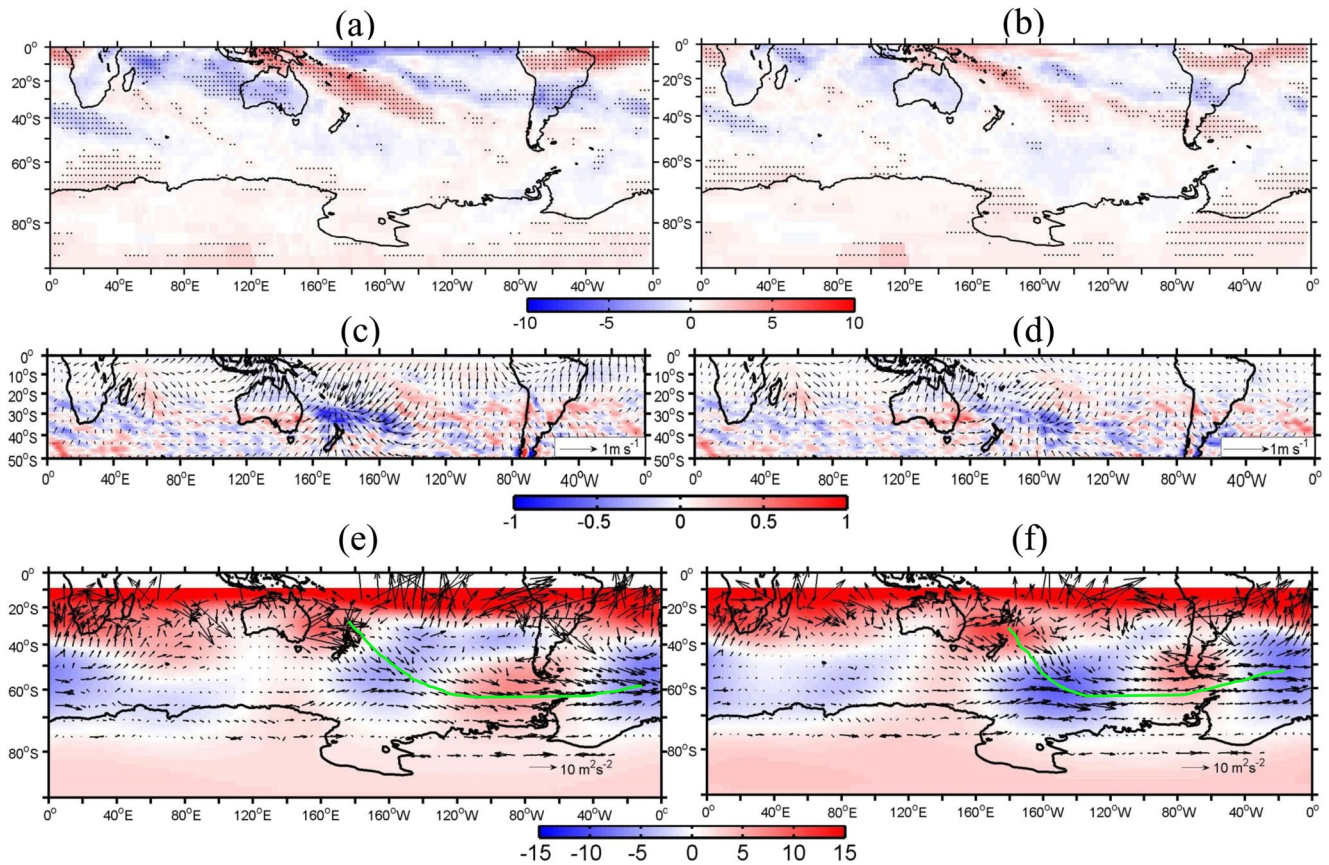


Figure 3. The same as Figure 2, but for outgoing longwave radiation (W m^{-2}) (a and b), Rossby wave source (shading) (10^{-10} s^{-2}) and 200-hPa divergent wind (vector) (c and d), wave activity flux (vector) and 200-hPa geopotential height (shading) (gpm) (e and f). The green thick lines indicate the propagation of the wavetrains.

anomalies related to the Niño3.4 index in austral spring show the largest influence on Antarctic sea ice (Figure S3d in Supporting Information S1).

In austral spring, the anomalous MSLP displays a spatial pattern similar to that of the Zonal Wave Three (Figure 4c). The positive MSLP anomalies over the Ross and Amundsen Seas suggest a weakened Amundsen Sea Low. These MSLP anomalies induce anomalous southerly winds over the Weddell and Bellingshausen Seas and anomalous northerly winds over the Amundsen and Ross Seas (Figure 4e). The anomalous southerly (northerly) winds correspond to decreased (increased) surface air temperature and positive (negative) sea ice concentration anomalies (Figures 4a and 4e). Without the ENSO signal, the MSLP anomalies are much smaller in magnitude (Figure 4d). In particular, there is no longer a large positive MSLP anomaly in the region of the Amundsen Sea Low. Significant sea ice anomalies only appear in the southwestern Pacific Ocean and the region north of the Antarctic Peninsula. The positive sea ice anomalies over the northern Weddell also are linked to the anomalous southerly winds there (Figure 4f).

The corresponding anomalous atmospheric circulation patterns for austral spring show a typical Pacific South America (PSA) mode over the Pacific sector of the Southern Ocean (Figure 5c). The OLR spatial pattern is a typical El Niño OLR pattern with increased (decreased) convective activity over the central and eastern tropical Pacific Ocean and western TIO (the eastern TIO and Maritime Continent). There are two wavetrains excited by the suppressed convection over the southwestern Pacific Ocean and the enhanced convection over the southwestern Indian Ocean (Figures 5a and 5e). The former propagates southeastward from the southwestern Pacific Ocean into the Bellingshausen and Weddell Seas. Large parts of the latter propagate northeastward into the eastern Indian Ocean; small parts of it propagate southeastward into East Antarctica. The anomalous wind and RWS also determine the origin of the wavetrains (Figure 5c). The anomalous convection activities over southeastern South America produce a wavetrain propagating northeastwards and southeastwards into the Indian Ocean

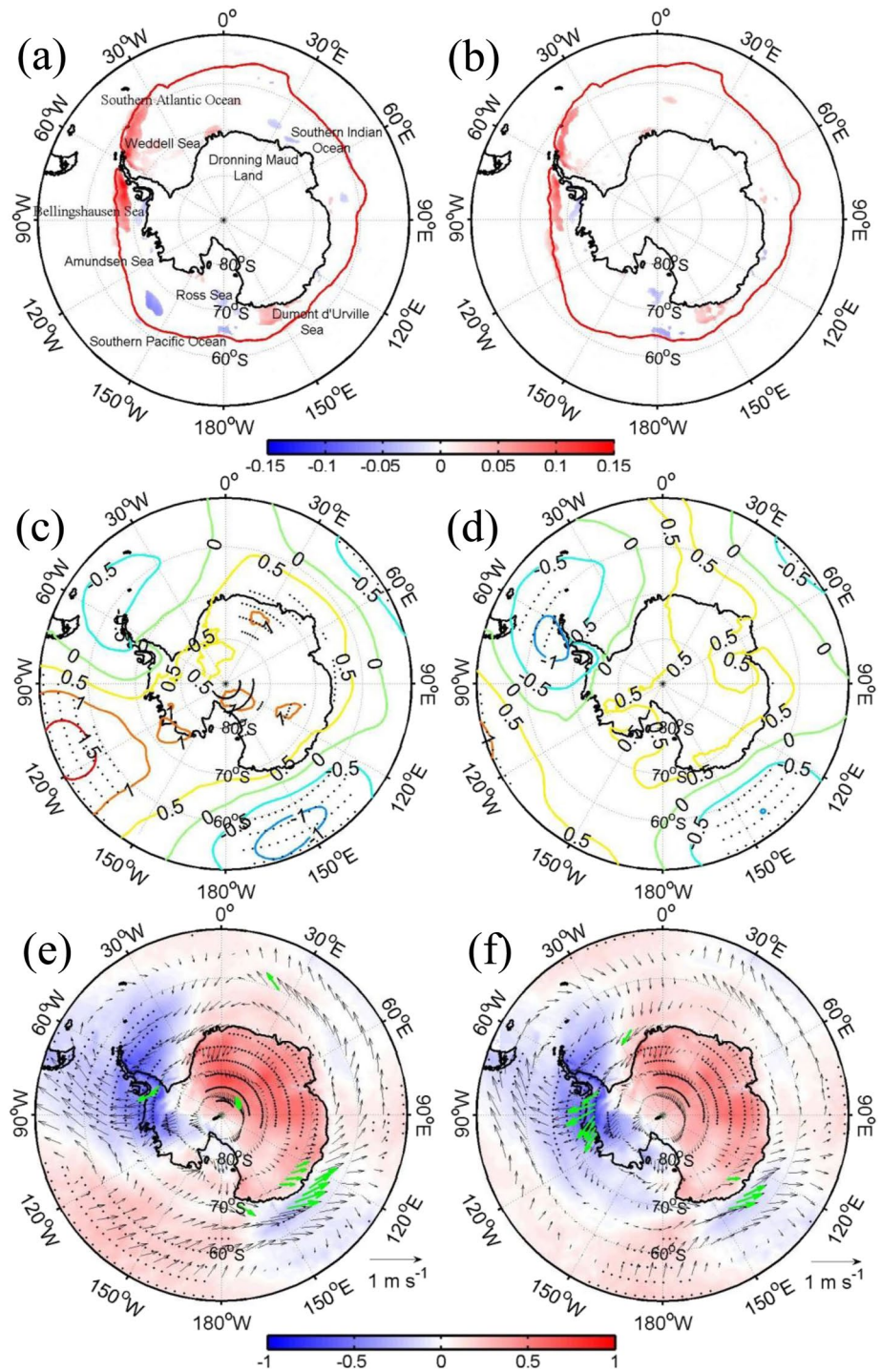


Figure 4. Regression map of anomalous seasonal sea ice concentration (a and b), mean sea level pressure (MSLP) (hectopascal) (c and d), and 10-m wind field (vector) and 2-m air temperature (°C) (e and f) onto the detrended Indian Ocean Basin Mode (IOBM) indices with the El Niño-Southern Oscillation (ENSO) signal (a, c and e) and without the ENSO signal (b, d and f) for austral spring over the 1979–2018 period. The Dipole Mode Index is removed from the detrended IOBM index. Only results at above 90% confidence levels are shown in panels (a and b). Dotted regions denote above 90% confidence level for MSLP and surface air temperature in panels (b, d, e and f). Green vectors denote above 90% confidence level in panels (e and f). The red thick lines in panels (a and b) denote the climatological sea ice extent (sea ice concentration is equal to 0.15).

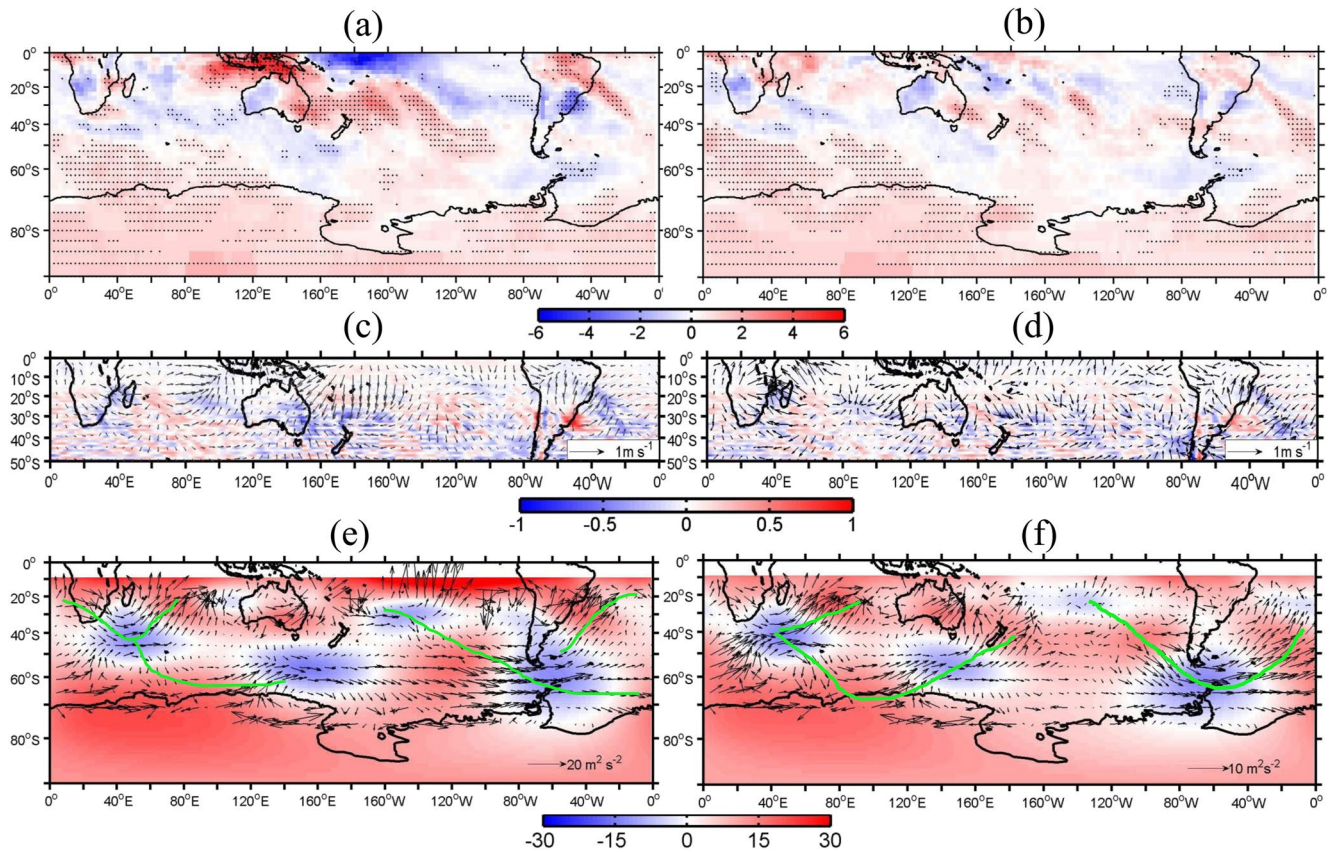


Figure 5. The same as Figure 4, but for outgoing longwave radiation (W m^{-2}) (a and b), Rossby wave source (shading) (10^{-10} s^{-2}) and 200-hPa divergent wind (vector) (c and d), wave activity flux (vector) and 200-hPa geopotential height (shading) (gpm) (e and f). The green thick lines indicate the propagation of the wavetrains.

(Figures 5a–5e). These wavetrains are related to the weakened Amundsen Sea Low and the PSA mode. The wavetrains are nearly opposite to those related to La Niña events (Wang et al., 2019), with a zonal shift related to the OLR difference. Without the ENSO signal, the PSA pattern disappears, but the Amundsen Sea Low is weakened slightly, though it is no longer statistically significant (Figure 5f). The positive OLR over the southwestern Pacific Ocean and negative OLR over the southeastern South America weaken, which result in the weaker wavetrains (Figure 5d). The wavetrain over the southwestern Indian Ocean strengthens and propagates southeastwards into the Southern Ocean, then northeastward into New Zealand (Figure 5f).

The sea ice anomalies related to the IOBM index in austral summer and winter are weaker than those in austral spring and autumn (Figure S5 in Supporting Information S1). In austral summer, the sea ice anomalies related to the positive IOBM with the ENSO signal display a dipole structure over the Ross Sea, with positive (negative) values over the eastern (western) Ross Sea (Figure S5a in Supporting Information S1). In addition, negative values also appear along the coastal region of Dronning Maud Land (Figure S5a in Supporting Information S1), which is expected as there is little sea ice far from the coast, except in the Weddell and Ross Seas. In austral winter, anomalies exist only in the northern margin of the sea ice zone with positive (negative) anomalies in the Weddell Sea (the southern Pacific Ocean) (Figure S5b in Supporting Information S1). In both summer and winter, the sea ice anomalies without the ENSO signal are smaller than with it (Figures S5c and S5d in Supporting Information S1). However, the extent of sea ice anomalies related to the Niño 3.4 index is smaller in austral winter and summer than in autumn and spring (Figures S2a and S2c in Supporting Information S1). The patterns of sea ice anomalies related to the IOBM with and without the ENSO signal in austral summer can be explained by anomalous MSLP, surface wind field and temperature, similar to what is observed in autumn and spring (Figures S6 and S7 in Supporting Information S1). The wavetrains excited by convective activity over the tropical

Indian and central Pacific Oceans propagate southeastwards into the Southern Ocean (Figures S8 and S9 in Supporting Information S1).

4. Conclusion and Discussion

In this study, we investigated whether there exists a teleconnection between the seasonal Antarctic sea ice concentration anomalies and the IOBM, one of the two dominant modes of SST anomalies in the TIO, and how the teleconnection, if exists, may be modulated by the presence or absence of ENSO.

The seasonal IOBM index is found to be correlated with the Niño 3.4 index, with the highest correlation in austral summer, followed by austral spring, and smallest in austral winter. Because the IOBM index is correlated with the DMI index in austral spring and winter, we use a new IOBM index with the DMI signal removed for these two seasons in our analyses. The linkage of the IOBM to Antarctic sea ice also depends on the season, with the largest areas of significant IOBM-related sea ice anomalies in austral autumn and spring and the smallest areas in winter. Especially in austral autumn and spring, positive sea ice anomalies occur in the Bellingshausen and northern Weddell Seas, and there are negative anomalies in the Amundsen Sea and the coastal seas off Dronning Maud land. Without the ENSO signal, the areal extent of the IOBM-related positive sea ice anomalies retreated substantially to the northern Weddell Sea in spring, and the extent of negative anomalies to the coastal region of East Antarctica in autumn and to the southwestern Indian Ocean in spring. Previous literature suggested that the IOBM peaks from austral summer to autumn (Chambers et al., 1999). However, the linkage between the IOBM and Antarctic sea ice is much weaker in summer than autumn.

Previous studies on the relationship between the variability of the Antarctic sea ice anomalies and the IOD, the other dominant TIO SST mode, also found a similar seasonal dependence (Nuncio & Yuan, 2015). We also examined the effect of the DMI on the Antarctic sea ice concentration for each season (Figure S10 in Supporting Information S1) and compared it to that of IOBM. For austral summer and autumn, the IOBM index has stronger connection to the Antarctic sea ice than the DMI index; the opposite is true for austral winter and spring.

With the ENSO signal, the convective activity anomalies over the tropical Pacific Ocean not only produce an additional wavetrain propagating into the Southern Ocean, but also enhance the magnitude of convective activity over the TIO. Without the ENSO signal, convective activity anomalies related to the IOBM can excite wave-trains, which produce atmospheric circulation anomalies over the Southern Ocean. Besides the Indian and Pacific Oceans, there are RWSs over the southeastern South America. Anomalous northerly (southerly) winds generate anomalous onshore (offshore) movement of sea ice, thus leading to decreased (increased) sea ice cover. Meanwhile, anomalous northerly (southerly) winds also transport warm (cold) and moist (dry) air, which increases (decreases) surface air temperature, thus reducing (expanding) sea ice cover.

Our study is, to our knowledge, the first to relate the IOBM index to the Antarctic sea ice variability on inter-annual time scale. Since the 1950s, SST in the TIO has been increasing at a rate of 0.1°C per decade (Dhame et al., 2020; Ihara et al., 2008; Lee et al., 2015; Luo et al., 2012). Whether this warming has contributed to Antarctic sea ice trends needs to be further examined. Further studies should also evaluate whether the IOBM-Antarctic sea ice relationship shows interdecadal variability, and if and how the relationship may be modified by the increase in the atmospheric greenhouse gas concentrations. Some idealized numerical experiments are needed to verify the relationships obtained through statistical methods and to separate the roles of the Indian and Pacific SST play in the relationships.

Data Availability Statement

The monthly Antarctic sea ice concentration data set is available from the (<http://nsidc.org/data/NSIDC-0051>). Monthly mean atmospheric variables are provided by ERA5 reanalysis (<https://www.ecmwf.int/en/forecasts/datasets/reanalysis-datasets/era5>). The monthly SST data in this study are derived from the NOAA Extended Reconstructed SST V5 (<https://psl.noaa.gov/data/gridded/data.noaa.ersst.v5.html>). The Niño3.4 index is available from the CPC, NOAA (<https://www.cpc.ncep.noaa.gov/data/indices/ersst5.nino.mth.91-20.ascii>). The OLR data are derived from the NOAA Interpolated OLR (http://psl.noaa.gov/data/gridded/data.interp_OLR.html).

Acknowledgments

We thank the European Centre for Medium-Range Weather Forecasts (ECMWF) for the ERA5 data. This study is financially supported by the National Science Foundation of China (41941009), the National Key R&D Program of China (2018YFA0605701), and the European Commission H2020 project Polar Regions in the Earth System (PolarRES; Grant 101003590).

References

Abram, N. J., Hargreaves, J. A., Wright, N. M., Thirumalai, K., Ummenhofer, C. C., & England, M. H. (2020). Palaeoclimate perspectives on the Indian Ocean Dipole. *Quaternary Science Reviews*, 237, 106302. <https://doi.org/10.1016/j.quascirev.2020.106302>

An, S. I. (2003). Conditional maximum covariance analysis and its application to the tropical Indian Ocean SST and surface wind stress anomalies. *Journal of Climate*, 16(17), 2932–2938. [https://doi.org/10.1175/1520-0442\(2003\)016<2932:CMCAAI>2.0.CO;2](https://doi.org/10.1175/1520-0442(2003)016<2932:CMCAAI>2.0.CO;2)

Chambers, D. P., Tapley, B. D., & Stewart, R. H. (1999). Anomalous warming in the Indian ocean coincident with El Niño. *Journal of Geophysical Research*, 104(C2), 3035–3047. <https://doi.org/10.1029/1998jc900085>

Delille, B., Vancoppenolle, M., Geilfus, N.-X., Tilbrook, B., Lannuzel, D., Schoemann, V., et al. (2014). Southern Ocean CO₂ sink: The contribution of the sea ice. *Journal of Geophysical Research: Oceans*, 119(9), 6340–6355. <https://doi.org/10.1002/2014JC009941>

De Souza, I. P., Andreoli, R. V., Kayano, M. T., Vargas, F. F., Cerón, W. L., Martins, J. A., et al. (2021). Seasonal precipitation variability modes over South America associated to El Niño–Southern Oscillation (ENSO) and non-ENSO components during the 1951–2016 period. *International Journal of Climatology*, 41(8), 4321–4338. <https://doi.org/10.1002/joc.7075>

Dhame, S., Taschetto, A. S., Santoso, A., & Meissner, K. J. (2020). Indian Ocean warming modulates global atmospheric circulation trends. *Climate Dynamics*, 55(7–8), 2053–2073. <https://doi.org/10.1007/s00382-020-05369-1>

Fogt, R. L., Bromwich, D. H., & Hines, H. M. (2010). Understanding the SAM influence on the South Pacific ENSO teleconnection. *Climate Dynamics*, 36(7–8), 1555–1576. <https://doi.org/10.1007/s00382-010-0905-0>

Gossart, A., Helsen, S., Lenaerts, J. T. M., Broucke, S. V., vanLipzig, N. P. M., & Souverijns, N. (2019). An evaluation of surface climatology in state-of-the-art reanalyses over the Antarctic Ice Sheet. *Journal of Climate*, 32(20), 6899–6915. <https://doi.org/10.1175/jcli-d-19-0030.1>

Hersbach, H., Bell, B., Berrisford, P., Hirahara, S., Horányi, A., Muñoz-Sabater, J., et al. (2020). The ERA5 global reanalysis. *Quarterly Journal of the Royal Meteorological Society*, 146(730), 1999–2049. <https://doi.org/10.1002/qj.3803>

Hobbs, W. R., Massom, R., Stammerjohn, S., Reid, P., Williams, G., & Meier, W. (2016). A review of recent changes in Southern Ocean sea ice, their drivers and forcings. *Global and Planetary Change*, 143, 228–250. <https://doi.org/10.1016/j.gloplacha.2016.06.008>

Hoskins, B. J., & Karoly, D. J. (1981). The steady linear response of a spherical atmosphere to thermal and orographic forcing. *Journal of the Atmospheric Sciences*, 38(6), 1179–1196. [https://doi.org/10.1175/1520-0469\(1981\)038<1179:TSLROA>2.0.CO;2](https://doi.org/10.1175/1520-0469(1981)038<1179:TSLROA>2.0.CO;2)

Huang, B., Thorne, P. W., Banzon, V. F., Zhang, H. M., Chepurin, G., Lawrimore, J. H., et al. (2017). Extended reconstructed sea surface temperature version 5 (ERSSTv5), upgrades, validations, and intercomparisons. *Journal of Climate*, 30(20), 8179–8205. <https://doi.org/10.1175/JCLI-D-16-0836.1>

Ihara, C., Kushnir, Y., & Cane, M. A. (2008). Warming trend of the Indian Ocean SST and Indian Ocean dipole from 1880 to 2004. *Journal of Climate*, 21(10), 2035–2046. <https://doi.org/10.1175/2007JCLI1945.1>

Kerr, R., Dotto, T. S., Mata, M. M., & Hellmer, H. H. (2018). Three decades of deep water mass investigation in the Weddell Sea (1984–2014): Temporal variability and changes. *Deep Sea Research Part II: Topical Studies in Oceanography*, 149, 70–83. <https://doi.org/10.1016/j.dsr2.2017.12.002>

Kidston, J., Taschetto, A. S., Thompson, D. W. J., & England, M. H. (2011). The influence of Southern Hemisphere sea-ice extent on the latitude of the mid-latitude jet stream. *Geophysical Research Letters*, 38(15), Artm L15804. <https://doi.org/10.1029/2011gl048056>

Klein, S. A., Soden, B. J., & Lau, N. C. (1999). Remote sea surface temperature variations during ENSO: Evidence for a tropical atmospheric bridge. *Journal of Climate*, 12(4), 917–932. [https://doi.org/10.1175/1520-0442\(1999\)012<0917:RSSTVD>2.0.CO;2](https://doi.org/10.1175/1520-0442(1999)012<0917:RSSTVD>2.0.CO;2)

Kwok, R., & Comiso, J. (2002). Spatial patterns of variability in Antarctic surface temperature: Connections to the southern Hemisphere annular mode and the southern oscillation. *Geophysical Research Letters*, 29(14), 1705. <https://doi.org/10.1029/2002GL015415>

Lee, S. K., Park, W., Baringer, M. O., Gordon, A. L., Huber, B., & Liu, Y. (2015). Pacific origin of the abrupt increase in Indian Ocean heat content during the warming hiatus. *Nature Geoscience*, 8(6), 445–449. <https://doi.org/10.1038/NNGEO2438>

Lefebvre, W., & Goosse, H. (2005). Influence of the southern annular mode on the sea ice-ocean system: The role of the thermal and mechanical forcing. *Ocean Science*, 1(3), 145–157. <https://doi.org/10.1029/2004JC002403>

Li, S., Lu, J., Huang, G., & Hu, K. (2008). Tropical Indian Ocean Basin warming and East Asian summer monsoon: A multiple AGCM study. *Journal of Climate*, 21, 6080–6088. <https://doi.org/10.1175/2008JCLI2433.1>

Liebmann, B., & Simth, C. A. (1996). Description of a complete (interpolated) outgoing longwave radiation dataset. *Bulletin of the American Meteorological Society*, 77, 1275–1277.

Luo, J.-J., Sasaki, W., & Masumoyo, Y. (2012). Indian Ocean warming modulates Pacific climate change. *Proceedings of the National Academy of Sciences of the United States of America*, 109(46), 18701–18706. <https://doi.org/10.1073/pnas.1210239109>

Massom, R. A., Scambos, T. A., Bennetts, L. G., Reid, P., & Stammerjohn, S. E. (2018). Antarctic ice shelf disintegration triggered by sea ice loss and ocean swell. *Nature*, 558(7710), 383–389. <https://doi.org/10.1038/s41586-018-0212-1>

McIntosh, P. C., & Hendon, H. H. (2017). Understanding Rossby wave trains forced by the Indian Ocean Dipole. *Climate Dynamics*, 50(7–8), 2783–2798. <https://doi.org/10.1007/s00382-017-3771-1>

Nuncio, M., & Yuan, X. (2015). The influence of the Indian Ocean Dipole on Antarctic sea ice. *Journal of Climate*, 28(7), 2682–2690. <https://doi.org/10.1175/JCLI-D-14-00390.1>

Ramon, J., Lledó, L., Torralba, V., Soret, A., & Doblas-Reyes, F. J. (2019). What global reanalysis best represents near-surface winds? *Quarterly Journal of the Royal Meteorological Society*, 145(724), 3236–3251. <https://doi.org/10.1002/qj.3616>

Raphael, M. N. (2007). The influence of atmospheric zonal wave three on Antarctic sea ice variability. *Journal of Geophysical Research*, 112(D12), D12112. <https://doi.org/10.1029/2006JD007852>

Riiheli, A., Bright, R. M., & Anttila, K. (2021). Recent strengthening of snow and ice albedo feedback driven by Antarctic sea-ice loss. *Nature Geoscience*, 14(11), 832–836. <https://doi.org/10.1038/s41561-021-00841-x>

Saji, N. H., Goswami, B. N., Vinayachandran, P. N., & Yamagata, T. (1999). A dipole mode in the tropical Indian ocean. *Nature*, 401, 360–363. <https://doi.org/10.1038/43854>

Sardeshmukh, P. D., & Hoskins, B. J. (1988). The generation of global rotational flow by steady idealized tropical divergence. *Journal of the Atmospheric Sciences*, 45(7), 1228–1251. [https://doi.org/10.1175/1520-0469\(1988\)045<1228:tgogr>2.0.co;2](https://doi.org/10.1175/1520-0469(1988)045<1228:tgogr>2.0.co;2)

Schott, F. A., Xie, S. P., & McCreary, J. P. (2009). Indian Ocean circulation and climate variability. *Reviews of Geophysics*, 47, RG1002. <https://doi.org/10.1029/2007RG000245>

Simpkins, G. R., Ciasto, L. M., Thompson, D. W. J., & England, M. H. (2012). Seasonal relationships between large-scale climate variability and Antarctic sea ice concentration. *Journal of Climate*, 25(16), 5451–5469. <https://doi.org/10.1175/jcli-d-11-003367.1>

Stammerjohn, S. E., Martinson, D. G., Smith, R. C., Yuan, X., & Rind, D. (2008). Trends in Antarctic annual Sea Ice retreat and advance and their relation to El Niño–Southern Oscillation and Southern Annular Mode variability. *Journal of Geophysical Research*, 113(C3), C03S90. <https://doi.org/10.1029/2007jc004269>

- Sun, B., Li, H., & Zhou, B. (2019). Inter decadal variation of Indian Ocean basin mode and the impact on Asian summer climate. *Geophysical Research Letters*, *46*(21), 12388–12397. <https://doi.org/10.1029/2019GL085019>
- Takaya, K., & Nakamura, H. (2001). A formulation of a phase in dependent wave-activity flux for stationary and migratory quasi geostrophic eddies on a zonally varying basic flow. *Journal of the Atmospheric Sciences*, *58*(6), 608–627. [https://doi.org/10.1175/1520-0469\(2001\)058<0608:AFOAPI>2.0.CO;2](https://doi.org/10.1175/1520-0469(2001)058<0608:AFOAPI>2.0.CO;2)
- Taschetto, A. S., & Ambrizzi, T. (2012). Can Indian Ocean SST anomalies influence South American rainfall? *Climate Dynamics*, *38*(7–8), 1615–1628. <https://doi.org/10.1007/s00382-011-1165-3>
- Taschetto, A. S., Gupta, A. S., Hendon, H. H., Ummenhofer, C. C., & England, M. H. (2011). The contribution of Indian Ocean sea surface temperature anomalies on Australian summer rainfall during El Niño events. *Journal of Climate*, *24*(14), 3734–3747. <https://doi.org/10.1175/2011JCLI3885.1>
- Turner, J., Hosking, J. S., Marshall, G. J., Phillips, T., & Barcegirde, T. J. (2016). Antarctic sea ice increase consistent with intrinsic variability of the Amundsen Sea Low. *Climate Dynamics*, *46*(7–8), 2391–2402. <https://doi.org/10.1007/s00382-015-2708-9>
- Uotila, P., Vihma, T., Pezza, A. B., Simmonds, I., Keay, K., & Lynch, A. H. (2011). Relationships between Antarctic cyclones and surface conditions as derived from high-resolution numerical weather prediction data. *Journal of Geophysical Research*, *116*(D7), D07109. <https://doi.org/10.1029/2010JD015358>
- Vihma, T., Johansson, M. M., & Launiainen, J. (2009). Radiative and turbulent surface heat fluxes over sea ice in the western Weddell Sea in early summer. *Journal of Geophysical Research*, *114*(C4), C04019. <https://doi.org/10.1029/2008JC004995>
- Wang, G., Hendon, H. H., Arblaster, J. M., Lim, E.-P., Abhik, S., & vanRensch, P. (2019). Compounding tropical and stratospheric forcing of the record low Antarctic sea-ice 2016. *Nature Communications*, *10*(1), 13. <https://doi.org/10.1038/s41467-018-07689-7>
- Xie, S. P., Hu, K., Hafner, J., Tokinaga, H., Du, Y., Huang, G., & Sampe, T. (2009). Indian Ocean capacitor effect on Indo-Western Pacific climate during the summer following El Niño. *Journal of Climate*, *22*(3), 730–747. <https://doi.org/10.1175/2008jcli2544.1>
- Xie, S. P., Kosaka, Y., Du, Y., Hu, K., Chowdary, J. S., & Huang, G. (2016). Indo-Western Pacific Ocean capacitor and coherent climate anomalies in post-ENSO summer: A review. *Advances in Atmospheric Sciences*, *33*, 411–432. <https://doi.org/10.1007/s00376-015-5192-6>
- Yang, J., Liu, Q., Liu, Z., Wu, L., & Huang, F. (2009). Basin mode of Indian Ocean sea surface temperature and Northern Hemisphere circumglobal teleconnection. *Geophysical Research Letters*, *36*(19), L19705. <https://doi.org/10.1029/2009GL039559>
- Yu, L., Zhong, S., Sui, C., Zhang, Z., & Sun, B. (2021). Synoptic mode of Antarctic summer sea ice superimposed on inter annual and decadal variability. *Advances in Climate Change Research*, *12*(2), 147–161. <https://doi.org/10.1016/j.accre.2021.03.008>
- Yu, L., Zhong, S., Vihma, T., Sui, C., & Sun, B. (2021). Sea ice changes in the Pacific sector of the Southern Ocean in austral autumn closely associated with the negative polarity of the South Pacific Oscillation. *Geophysical Research Letters*, *48*(7), e2021GL092409. <https://doi.org/10.1029/2021GL092409>
- Yu, L., Zhong, S., Zhou, M., Sun, B., & Lenschow, D. H. (2018). Antarctic summer sea ice trend in the context of high latitude atmospheric circulation changes. *Journal of Climate*, *31*(10), 3909–3920. <https://doi.org/10.1175/JCLI-D-17-0739.s1>
- Yuan, X. (2004). ENSO-related impacts on Antarctic sea ice: A synthesis of phenomenon and mechanisms. *Antarctic Science*, *16*(4), 415–425. <https://doi.org/10.1017/s0954102004002238>
- Zhang, Z., Uotila, P., Stössel, A., Vihma, T., Liu, H., & Zhong, Y. (2018). Seasonal southern Hemisphere multi-variable reflection of the southern annular mode in atmosphere and ocean reanalyses. *Climate Dynamics*, *50*(3–4), 1451–1470. <https://doi.org/10.1007/s00382-017-3698-6>